The roles of conduit redundancy and connectivity in xylem hydraulic functions

Assaad Mrad[1,2,3,6], Daniel M Johnson[4], David M Love[4], and Jean-Christophe Domec[1,5]

[1] *Nicholas School of the Environment, Duke University, Durham, NC 27708, USA*
[2] *Department of Civil and Environmental Engineering, University of California, Irvine, CA 92697, USA*
[3] *Department of Engineering, Wake Forest University, Winston-Salem, NC 27101, USA*
[4] *Warnell School of Forestry and Natural Resources, University of Georgia, Athens, GA 30602, USA*
[5] *Bordeaux Sciences Agro, UMR 1391 INRA-ISPA, 33175 Gradignan Cedex, France*
[6] *Corresponding author: mradassaad2@gmail.com, +1-919-519-0011*

Figs. 1, 2, 3, 4, 8, and 9 to be published in color

Assaad Mrad - ORCID: https://orcid.org/0000-0003-4922-4446 - twitter: @mradassaad
Daniel M Johnson - ORCID: https://orcid.org/0000-0003-1015-9560 - twitter: @TreePhysDJ
David M Love - no ORCID
Jean-Christophe Domec - ORCID: https://orcid.org/0000-0003-0478-2559

Total word count (excluding summary, references and legends):	6637
Summary	199
Introduction	1393
Description	2492
Results	1297
Discussion	1455
Acknowledgements	34
Number of figures	9
Number of tables	0
Number of supporting files	5 (Figs. S1-S3, Description S1-S2)

This article has been accepted for publication and undergone full peer review but has not been through the copyediting, typesetting, pagination and proofreading process, which may lead to differences between this version and the Version of Record. Please cite this article as doi: 10.1111/NPH.17429

1 Summary

1. Wood anatomical traits shape a xylem segment's hydraulic efficiency and embolism spread resistance due to declining water potential. It has been known for decades that variations in conduit connectivity play a role in altering xylem hydraulics. However, evaluating the precise effect of conduit connectivity has been elusive. The objective is to establish an analytical linkage between conduit connectivity and grouping and tissue-scale hydraulics.

2. It is hypothesized that an increase in conduit connectivity brings improved resistance to embolism spread due to increased hydraulic pathway redundancy. However, an increase in conduit connectivity could also reduce resistance due to increased embolism spread speed with respect to pressure. We elaborate on this trade-off using graph theory, percolation theory, and computational modeling of xylem. The results are validated using anatomical measurements of *Acer* branch xylem.

3. Considering only species with vessels, increases in connectivity improve resistance to embolism spread without negatively affecting hydraulic conductivity. The often measured grouping index fails to capture the totality of the effect of conduit connectivity on xylem hydraulics.

4. Variations in xylem network characteristics, such as conduit connectivity, might explain why hypothesized trends among woody species, like the 'safety-efficiency' trade-off hypothesis, are weaker than expected.

Keywords: connectivity, grouping, xylem, hydraulic conductance, embolism spread, *Acer* (Maples)

2 Introduction

Plant xylem supplies water from the soil pores to the leaves to compensate for the loss of water molecules from leaves to the atmosphere. As stomata open to uptake

carbon dioxide molecules needed for photosynthesis, water molecules evaporate. The water experiences a phase transition in the leaf parenchyma and escapes as vapor through the guard cells to a desiccating atmosphere. For every water molecule lost from leaves, the entire column of water must be pulled upwards from the soil-root interface or from plant water storage to compensate for this water molecule loss. This makes the conveyance of water from roots to leaves through the xylem is unique; it is entirely passive with minimal energy expenditures (no pumping) and operationally relies on water loss from leaves via transpiration only (Venturas, Sperry, and Hacke, 2017). However, the draw-back of such a passive system is that water in the xylem is in a metastable state where cohesive forces between water molecules and adhesive forces between the molecules and the cell walls sustain large tensile stresses (Dixon and Joly, 1895). This tension is then transmitted to the xylem cell walls and sap.

The xylem tissue bears a complex network of sap-transporting conduits that form many parallel pathways for water movement. The network of conduits, extending from the roots to the leaves, is redundant such that if a conduit is damaged, many other pathways still exist for the water to reach the leaves. The water is able to move from one conduit to the next through interconduit pits (hereafter "pits"), which are openings in the secondary cell wall of conduits that allow lateral water transport. Pathway redundancy in xylem is necessary because conduits are often at the risk of dysfunction through gas bubble expansion.

The consequence of having sap under tension in a conduit is that some gas-filled bubbles can grow and fill the whole conduit. Embolisms inside conduits have been hypothesized to originate and spread through homogeneous nucleation, heterogeneous nucleation from a crack or impurities, or air-seeding from porous pits on conduit walls (Tyree, Davis, and Cochard, 1994). In the angiosperm clade, of main interest in this study, the pits contain a porous membrane, termed the pit membrane, that links conduits to each other. Pressure chamber experiments have lent support to the hypothesis of air-seeding via pores in the interconduit pit membranes by demonstrating the equivalence between a drop in sap pressure and a rise in the pressure of embolism contents (Cochard, Cruiziat, and Tyree, 1992; Sperry and Saliendra, 1994). This is because nucleation, or cavitation, requires negative water pressures

to occur whereas air-seeding is dependent on the absolute value of the pressure difference between the gas in embolized vessels and the sap (P). Air-seeding from adjacent conduits is considered the sole source of embolisms in this study. In other words, when a conduit is embolized, or air-filled, there is risk for embolism to spread to adjacent, connected conduits (Sperry and Tyree, 1988). This requires an initial embolism event as exposure of the xylem sap to air due to disturbances like fire and strong winds, herbivores, or pathogens (Venturas, Sperry, and Hacke, 2017) or de novo heterogenous nucleation. These initial embolisms might then spread to a larger number of vessels through air-seeding.

The ultimate impact of vessel embolism is related to its effect on organ and whole-plant hydraulic function. When a functional vessel is air-filled, at least one hydraulic pathway from segment inlet to outlet is lost, affecting whole-segment hydraulics. The way vessels are distributed and connected to one another determines the degree to which an embolism affects segment-level resistance to embolism spread. One such measure is the vulnerability to embolism curve (VC): a plot of the percent loss of hydraulic conductivity (PLC) of a whole-segment against P (Tyree and Zimmermann, 2002). As P increases, the PLC increases from 0% to 100%. The shape and location of the VC along the P axis depends on embolism spread within the xylem network of that segment, the ease of which is determined by pit membrane ultra-structural properties and frequency.

However, being a 'macro-scale' measure, the VC integrates network mechanisms beyond vessel to vessel embolism exchange. Examples of these mechanisms are the redundancy of the xylem hydraulic pathway (F. Ewers, J. Ewers, Jacobsen, and López-Portillo, 2007), the variability of conduit wall susceptibility to embolism spread along the segment cross-section (Venturas, Pratt, Jacobsen, V. Castro, Fickle, and Hacke, 2019), patterns of disease epidemics on graphs (Roth-Nebelsick, 2019), and the so-called percolation threshold. The percolation threshold is an effective 'seal' against un-inhibited embolism spread born out of vessel connectivity statistics (Callaway, Newman, Strogatz, and Watts, 2000). As of yet, the percolation threshold has never been utilized in the literature to infer VCs. It is a network property that links the speed of disease, or embolism, spread in a network based on the connectivity (number

of neighbours) of the agents (vessels). It is these 'mid-scale' mechanisms, straddling the 'micro-scale' processes and 'macro-scale' measures, that are of interest and frame the scope of the work here.

The basic property that controls xylem pathway redundancy and embolism 'percolation' is the average vessel connectivity ($\langle c \rangle$). The average vessel connectivity in a xylem segment is the number of vessel neighbors (i.e., with a common contact wall providing hydraulic connection), averaged over all vessels in the xylem segment (Loepfe, Martinez-Vilalta, Pinol, and Mencuccini, 2007; Martínez-Vilalta, Mencuccini, Álvarez, Camacho, Loepfe, and Piñol, 2012; Newman, 2018). Unfortunately, $\langle c \rangle$ has rarely been reported in the literature but the grouping index (GI) is a measure commonly quantified by anatomists (Carlquist, 1984). The GI is the number of vessels in a xylem cross-section divided by the number of vessel groups. Therefore, the GI is a two-dimensional proxy to $\langle c \rangle$. To make use of the GI and link it to $\langle c \rangle$, we focus on a particular type of wood.

The interest here is in angiosperm species that lack vasicentric tracheids (Carlquist, 1984; Pratt and Jacobsen, 2018). Flowering plants with vasicentric tracheids can achieve pathway redundancy by surrounding vessels by tracheids (Hacke, Jacobsen, and Pratt, 2009; Pratt, Percolla, and Jacobsen, 2015). While vasicentric tracheids are dramatically smaller in diameter and length, they could be numerous enough to sustain significant 'back-up' flow in case an adjacent vessel is embolized (Sano, Morris, Shimada, Ronse De Craene, and Jansen, 2011). When anatomists report measures of vessel grouping such as the GI, they only count vessels and disregard tracheids. Therefore, by focusing on species lacking vasicentric tracheids, we purposely take advantage of data representing the true connectivity of the xylem hydraulic pathway. Particularly, we will be utilizing data on seven species of the genus *Acer* (Lens, Sperry, Christman, Choat, Rabaey, and Jansen, 2011) that belongs to the Sapindaceae family, generally lacking vasicentric tracheids (Carlquist, 1984).

The plant physiology literature has made significant strides in understanding the linkages between vessel (Hacke, Sperry, Wheeler, and L. Castro, 2006; Christman, Sperry, and Adler, 2009; Christman, Sperry, and Smith, 2012) and pit anatomy (Choat, Cobb, and Jansen, 2008; Jansen, Choat, and Pletsers, 2009; Lens, Sperry,

Christman, Choat, Rabaey, and Jansen, 2011; Li, Lens, Espino, Karimi, Klepsch, Schenk, Schmitt, Schuldt, and Jansen, 2016), vessel to vessel air-seeding, and whole segment resistance to embolism spread through the VC. But processes mediated by xylem network properties (Jacobsen and Pratt, 2018) have received relatively less attention and are still elusive because pertinent measurements are lacking. Xylem network theory (F. Ewers, J. Ewers, Jacobsen, and López-Portillo, 2007) and modeling (Loepfe, Martinez-Vilalta, Pinol, and Mencuccini, 2007; Martínez-Vilalta, Mencuccini, Álvarez, Camacho, Loepfe, and Piñol, 2012; Mrad, Domec, Huang, Lens, and Katul, 2018) provide viable avenues for investigating these processes. As long as the effect of the xylem network is unclear, opportunities to link anatomy and segment hydraulics and to generalize trends among plant species will be missed. How the xylem network and vessel connectivity affect whole-segment hydraulics and resistance to embolism spread is here investigated through a synergistic combination of three-dimensional xylem computer modeling and graph theory.

In what follows, we outline the modeling and theory employed and compare the analytical linkage between average vessel connectivity and xylem hydraulics to anatomical measurements of *Acer* xylem. We present an extension to a xylem hydraulic model (Mrad, Domec, Huang, Lens, and Katul, 2018) to simulate Maple branch xylem segments by matching certain measurements of xylem network structure. With the aid of the model and graph theory, we link xylem vessel anatomy and connectivity to xylem VC measures and hydraulic conductivity. Ultimately, we highlight that increasing vessel connectivity increases the magnitude of the 'air-entry' pressure of xylem segments, without compromising hydraulic efficiency. Then, we put these results in the context of Maple xylem and the 'safety-efficiency' trade-off hypothesis.

3 Description

The two-dimensional (2D) model presented in Mrad, Domec, Huang, Lens, and Katul (2018) is extended by introducing a three-dimensional (3D) representation. The radial dimension is added to the model such that 3D growth ring sections are simulated. In

its new form, the model is suited for diffuse-porous angiosperm xylem where conductive, vasicentric tracheids are absent or play a minimal role in total tissue hydraulics. In the following, the anatomical elements represented in the model are only briefly described because of significant overlap with the description in Mrad, Domec, Huang, Lens, and Katul (2018). In contrast, aspects of the model related to 3D representation of xylem networks are extensively explained.

Throughout, water is assumed to be incompressible and its properties, including viscosity and density, are constant and defined at 25^oC and standard pressure. Water flow in all vessels is assumed to be laminar. Each vessel is represented by a vertical cylinder with diameter D_v and length L_v. The vessel lumens are hydraulically connected by intervessel connection (IVC). The IVCs link adjacent vessel elements along the radial or tangential directions. Every vessel has a specified contact wall area determined by the vessel contact fraction (f_c) and the vessel cylindrical wall area (A_v). The ensemble of all IVCs between two vessels constitute their contact wall. The contact wall is divided into a pit-field area using the pit-field area fraction (f_{pf}) such that the pit-field area of each vessel equals $A_v \times f_c \times f_{pf}$. The pit-field area of each contact wall contains the pits and its size determines the number of pit membranes it contains. The interest here is in the average of vessel or pit properties throughout a xylem segment denoted using the $\langle$property$\rangle$ notation. The aforementioned anatomical properties have been measured on seven *Acer* species in Lens, Sperry, Christman, Choat, Rabaey, and Jansen (2011).

3.1 Modeling xylem networks: sap flow

To calculate the sap flow across a xylem segment, it is necessary to determine the flow through vessel elements and IVCs. Water flow through vessel lumens is described by the Hagen-Poiseuille equation while sap flow through IVCs is described by a superposition of Sampson and Hagen-Poiseuille flow resistances (Description S1).

The $k_{xa,max}$ of a modeled xylem segment is then calculated. $k_{xa,max}$ is the maximum xylem area-normalized hydraulic conductivity of a segment. $k_{xa,max}$ is estimated by solving an equivalent hydraulic resistor network subject to a pressure difference between its ends (Description S1). The resistances of the vessel elements and IVCs follow the equations above. One end of the segment is set at a given pressure, say atmospheric pressure, while the other end is subject to a higher pressure to form a pressure difference ΔP_{seg}. Then,

we establish a set of linear equations to be solved simultaneously like an electric resistor circuit (Mrad, Domec, Huang, Lens, and Katul, 2018). The set of equations consist of the Hagen-Poiseuille and Sampson flow equations mentioned in the previous paragraph for every vessel element and IVC (Description S1). The solution of the set gives the sap flow through the segment Q_{seg}. The hydraulic conductance of the segment (K_{seg}) is then estimated as

$$K_{seg} = \frac{Q_{seg}}{\Delta P_{seg}}. \tag{1}$$

Additionally, $k_{xa,max}$ is

$$k_{xa,max} = \rho \frac{L_{seg}}{A_{seg}} K_{seg}, \tag{2}$$

where L_{seg} and A_{seg} are respectively the axial length of the simulated segment and its transverse area while ρ is the density of pure water.

3.2 Modeling xylem networks: embolism spread

Air-seeding requires embolism spread to originate from an adjacent vessel through one of the pits connecting two vessels (Tyree and Zimmermann, 2002). An embolism spreads to an adjacent vessel when the absolute value of the pressure difference between the air inside the embolism and the surrounding sap (P) exceeds the capillary pressure i.e., the air-seeding pressure (ASP) of the contact wall connecting two vessels.

In angiosperms, pit membrane anatomy and frequency throughout vessel wall surfaces determine the critical P at which air-seeding occurs. By restricting the gas bubble meniscus to sizes of the order of nanometers, pit membranes reduce the chance that the bubble will spread from the embolized vessel and fill the functional one. The growth of the bubbles is dictated by their size, the number of gas molecules in them, and their surface chemistry (Schenk, Espino, Romo, Nima, Do, Michaud, Papahadjopoulos-Sternberg, Yang, Zuo, Steppe, et al., 2017; Konrad, Katul, Roth-Nebelsick, and Jensen, 2019; Kanduč, Schneck, Loche, Jansen, Schenk, and Netz, 2020). However, analytical relations linking pit structural properties and their function in blocking air-seeding are lacking. Difficulties encompass the formation of lipid-coated nanobubbles that allow for stable bubbles to exist in functional vessels (Schenk, Steppe, and Jansen, 2015; Schenk, Espino, Romo, Nima, Do, Michaud, Papahadjopoulos-Sternberg, Yang, Zuo, Steppe, et al., 2017) and the presence of a rare and leaky pit (Christman, Sperry, and Adler, 2009). Measurements of pit

membrane structure are thought to suffer from artefacts introduced through sample preparation and dehydration (Li, Lens, Espino, Karimi, Klepsch, Schenk, Schmitt, Schuldt, and Jansen, 2016). Moreover, the exact link between pit membrane anatomy and function is not complete as of yet due to the complex interactions between its 3D structure and existing chemical compounds (Kaack, Altaner, Carmesin, Diaz, Holler, Kranz, Neusser, Odstrcil, Schenk, Schmidt, et al., 2019; Zhang et al., 2020).

Therefore, the effects of these pit traits on embolism spread resistance is surrogated to a pit ASP distribution. This distribution surrogates the complexity of the pit membrane ultra-structure including thickness, pore size, quantity, and chemistry. The pit membrane ASPs are sampled from a two-parameter Weibull distribution that differs among species (Christman, Sperry, and Adler, 2009). This distribution is given by (Christman, Sperry, and Adler, 2009)

$$F_m(ASP) = 1 - exp\Big[- \Big(\frac{ASP}{a} \Big)^b \Big], \tag{3}$$

where a and b are distribution parameters and $F_m(ASP)$ is the cumulative distribution function of pit membrane ASPs.

Embolisms spread through the leakiest membrane between two vessels (Christman, Sperry, and Adler, 2009). To account for this 'extreme-value' effect, the cumulative distribution function of ASP for a contact wall containing N_m pit membranes is derived from an extreme-value distribution as (Mrad, Domec, Huang, Lens, and Katul, 2018)

$$F_c(ASP) = 1 - [1 - F_m(ASP)]^{N_m} = 1 - exp\Big[- \Big(\frac{ASP}{a/N_m^{1/b}} \Big)^b \Big]. \tag{4}$$

In other words, $F_c(ASP)$ is the probability that a given P will exceed the ASP of a randomly chosen contact wall in the xylem network. Therefore, larger contact walls in the same xylem segment are more likely to have a leakier pit. Air-seeding is assumed to result in unstable bubbles that fill up the 'infected' vessel completely and instantaneously, rendering it non-functional. This simplification is plausible as unstable bubbles expand rapidly (in micro-seconds; Konrad and Roth-Nebelsick, 2003; Hölttä, Vesala, and Nikinmaa, 2007). Such an idealization also eliminates the need to represent the aerodynamics of air expansion within a vessel and any concomitant interaction with water movement.

Having assigned each contact wall an ASP, the vulnerability to embolism curve (VC) of the simulated growth ring section can be computed. An embolism is injected into random

vessels inside the network. Then, the pressure of its contents is increased at successive steps while the water pressure is maintained at P_{atm} akin to the air-injection technique (Salleo, Hinckley, Kikuta, Lo Gullo, Weilgony, Yoon, and Richter, 1992). After every increase in P, the initial random embolism could spread to other conduits based on the adjacent contact wall ASPs. At every step, with some conduits embolized and non-functional, the unsaturated xylem area-specific hydraulic conductivity (k_{xa}) is computed. Then the percent loss in hydraulic conductivity (PLC) is determined as

$$\mathrm{PLC}(P) = 100 \times \left(1 - \frac{k_{xa}(P)}{k_{xa,max}}\right). \tag{5}$$

The VC is the curve plotting PLC against increasing P. For the ensuing analysis, P_{50} is defined as the absolute value of pressure at which $\mathrm{PLC}(P_{50}) = 50$. Similarly, P_{88} and P_{12} are defined at $\mathrm{PLC}(P_{88}) = 88$ and $\mathrm{PLC}(P_{12}) = 12$, respectively (Domec and Gartner, 2001). *In planta*, water is under tension and therefore is under negative pressure. Here, we look at the absolute values of those pressures.

3.3 Modeling xylem networks: implementation of *Acer* hydraulics and 3D structure

To ensure the simulated xylem networks model real tissues, several anatomical and connectivity-related measurements parameterize the simulated segments as elaborated in this section. The measured average vessel length $\langle L_v \rangle$ and diameter $\langle D_v \rangle$, f_c and f_{pf} for each species are used as inputs of the 3D version. These model inputs ensure that water flow resistance through vessels and the frequency of contact walls and pit-field areas are realistic. $\langle D_v \rangle$ and f_{pf} are used to model the number of pit membranes per contact wall.

In addition to the 2D version, the 3D version of the model employs two measurements to realistically represent the connectivity and frequency of vessels in the segment. The GI equals the number of vessels in a xylem cross-section divided by the number of vessel groups which also include solitary vessels (Carlquist, 1984) and the vessel frequency (VA_x^{-1}) equals the number of vessels per unit transverse xylem area (Fig. 1). The model employs both measures to tune frequency of vessels in the 3D xylem segment, the probability of a radial IVC with an adjacent vessel, and the probability of a tangential IVC. The majority of IVCs in *Acer* are radial so we constrain the probability of tangential connections

within 5% and 20%. This interval is liberal and encompasses the estimated proportions of tangential connections of the *Acer* segments based on their cross-sectional images (Fig. 1). Model simulations show that the proportion of tangential connections alone is insufficient to explain variation in $k_{xa,max}$ and P_{50} among species (Fig. S1). Therefore, constraining the proportion of tangential connections to a liberal range will faithfully represent xylem conduit geometry while not reducing the generality of this study's conclusions. Because of this constraint, the probability of radial connections and the probability of vessel initiation are now determined using these two independent measurements: GI and VA_x^{-1} (Description S2).

In Fig. 1, the xylem model ensures that vessel connectivity patterns in a modeled growth ring section matches those in an *Acer negundo* section. The modeled ring cross-section shows vessel lumen of varying diameters (not represented) as colored dots. Those that are connected by an IVC have a red line connecting them (Fig. 1a). Vessels of the same color are hydraulically connected (Mrad, Domec, Huang, Lens, and Katul, 2018). In the simulated segment, two vessels appearing disconnected in that transverse section does not preclude them being connected at another axial location.

Fig. 1a highlights three vessel groups with a correspondence to a group in an *Acer negundo* imaged ring (Fig. 1b). The black and white rectangles show vessel groups with connections that are uniquely radial while the ellipses and hexagons have a single diagonal connection each. This highlights how the model recovers the preferential direction of vessel connections in the *Acer* genus.

In this article, the pit membrane hydraulic parameters are fitted to obtain agreement with tissue-level hydraulic measurements because theoretical links between anatomy, hydraulic conductivity, and embolism spread resistance are uncertain as explained above. For example, pore diameter is fit such that $k_{xa,max}$ of the whole xylem segment matches the measurements. Similarly, the two parameters, a and b, of $F_m(ASP)$ (equations 3 and 4) were tuned such that the modeled VC was similar to the measured VC through P_{12}, P_{50}, and P_{88} (Fig. 1, c). The match was not evaluated more rigorously because the results of this study do not depend on it.

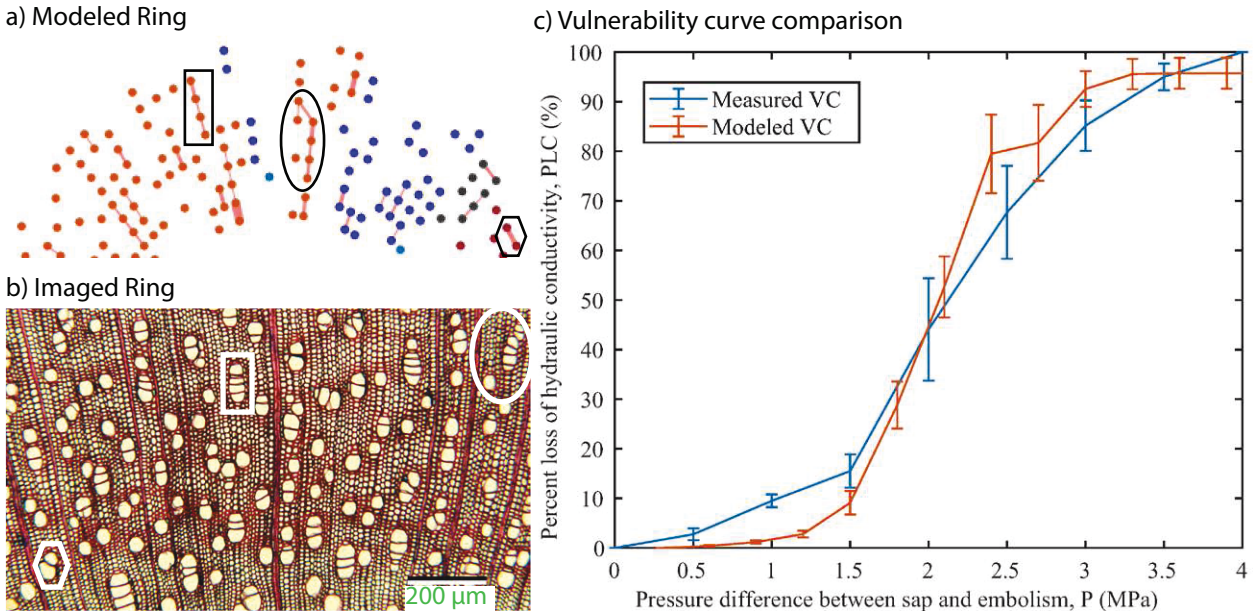

Fig. 1 Illustration showing the correspondence between a) a cross-sectional view of a modeled *Acer negundo* ring and b) an image of an *Acer negundo* branch and c) the resulting vulnerability to embolism curves (VC). The model does not represent each vessel in the image but approximates the averaged anatomy and xylem network properties. Three corresponding elements are highlighted by two rectangles, two ellipses, and two hexagons. The rectangles show a uniquely radial file of vessels, the ellipses show a vessel group dominated by radial connections but with the occasional tangential or diagonal connection, and the hexagons show two vessels connected diagonally. Both the modeled and imaged rings have a grouping index of 1.84 and a vessel density of 263 mm^{-2} (Lens, Sperry, Christman, Choat, Rabaey, and Jansen, 2011). Similarly colored vessels are members of the same hydraulic component (see Description). The error bars around the measured and modeled VCs represent standard errors resulting from 6 *Acer* negundo branches (blue) and 10 simulated branches (red).

3.4 Theory

Diffuse-porous species exemplified by *Acer* have quasi-uniform anatomical properties from earlywood to latewood. As a result, only vessel connectivity is of interest here. The simulated xylem segments keep average anatomical traits stationary throughout a growth ring.

Three-dimensional xylem is represented by a graph of nodes connected to each other via edges as in Fig. 2. We collapse each vessel onto a node as shown in the correspondence between vessels in Fig. 2a and nodes in Fig. 2b. The edges represent contact walls. A node has one of two states: functional or embolized. This representation of xylem is used to characterize embolism spread. Each edge in the graph representation is weighted by its ASP. As P increases, it exceeds a higher fraction of edge ASPs (i.e., $F_c(P)$ is an increasing function of P) so more edges become conducive to embolism spread if one exists adjacently.

The number of vessels a given vessel is connected to is called its connectivity c. For example, vessel 3 in Fig. 2 has $c_3 = 3$ and vessel 4 has $c_4 = 1$. Of main interest is the average connectivity of the xylem network $\langle c \rangle$ over all its constituent vessels. The primary role of $\langle c \rangle$ in hydraulic pathway redundancy and extent of embolism propagation throughout the xylem network is now considered.

As alluded to above, at a given P a fraction $F_c(P)$ of vessel to vessel edges are amenable to disease spread. In network or graph theory parlance, it is said that these edges are 'occupied'. Given these definitions, the process of embolism spread on xylem vessel networks falls under the realm of edge percolation processes on a graph (Callaway, Newman, Strogatz, and Watts, 2000; Newman, 2018). Percolation processes stipulate a threshold fraction of 'occupied' edges $F_{c,threshold}$ where, if $F_c(P) > F_{c,threshold}$, it is expected that an embolism, randomly placed in the xylem network, will spread to the majority of the network. In other words, the percolation threshold is a limit on the fraction of contact walls with an ASP below the pressure difference between sap and bubble contents (P). When the threshold is exceeded, a randomly placed embolism is expected to spread to the majority of a xylem network. In a class of graphs applicable to xylem, called configuration models, the percolation threshold $F_{c,threshold}$ depends solely on the first $\langle c \rangle$ and second $\langle c^2 \rangle$ moments of the vessel connectivity distribution

$$F_{c,threshold} = \frac{\langle c \rangle}{\langle c^2 \rangle - \langle c \rangle}. \tag{6}$$

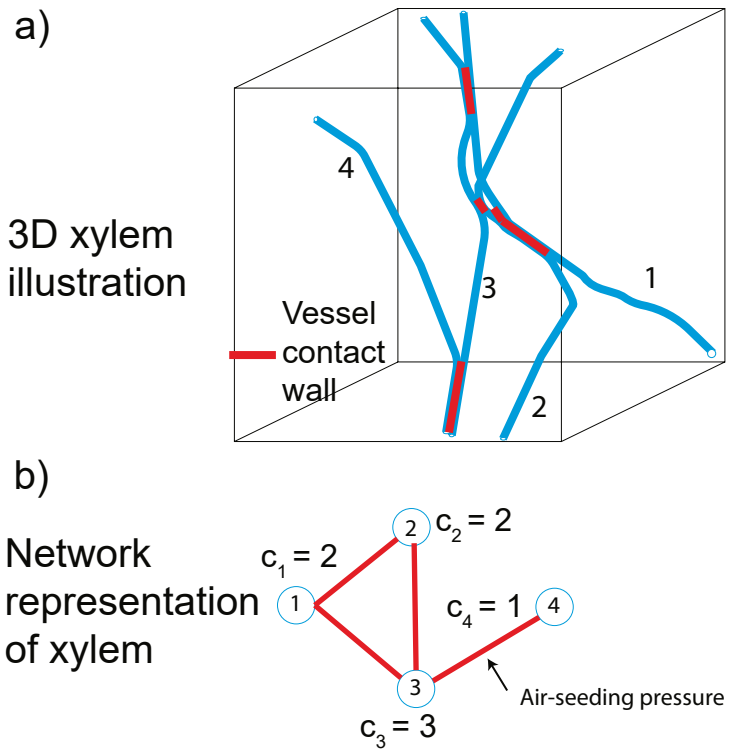

Fig. 2 Illustration of a) a three-dimensional xylem network connected via contact walls, and b) the connectivities (c1-c4) of those conduits for embolism spread purposes. Every vessel (blue) in the xylem is collapsed onto a node while vessel contact walls (red) are represented by a bi-directional edge connecting the nodes. Every edge is weighted by the air-seeding pressure of the contact wall connecting the vessels. The length of each edge as drawn in b) does not represent any property. The connectivity of every node in sub-figure b) is shown next to it. The average vessel connectivity of this example is $\langle c \rangle = 2$.

This result was first reported in a study of "the resilience of the Internet to random breakdowns" (Cohen, Erez, Ben-Avraham, and Havlin, 2000). Because percolation theory concerns graphs of infinite size and the xylem network is necessarily finite, the actual $F_{c,threshold}$ is expected to be smaller than its theoretical value (equation 6) due to 'finite-size' effects.

The direct consequence of vessel connectivity on a species' cavitation resistance is not straightforward and involves a trade-off explained in the Results. Determining the functional significance of vessel grouping is further complicated because pit structure (i.e., pit membrane thickness and pit chamber depth) and connectivity (i.e., GI and $\langle L_v \rangle$) co-vary (Lens, Sperry, Christman, Choat, Rabaey, and Jansen, 2011). Such co-variations could lead to unexpected emergent tissue hydraulic behavior that is suited to a mechanistic exploration and which we address next.

3.5 Varying vessel anatomy and connectivity

Simulations were performed in which VA_x^{-1}, $\langle L_v \rangle$, $\langle D_v \rangle$ are varied as well as the probabilities of radial and tangential connections to adjacent vessels. Such variations perturbed GI and $\langle c \rangle$. As these model properties were varied, others such as pit membrane diameter and the contact wall ASP distribution $F_c(ASP)$, which affect embolism spread resistance (equation 4), were kept constant. In other words, the distribution function's parameters a and b are varied such that $F_c(ASP)$ is independent of N_m between simulations (equation 4). This allows disentangling the effect of vessel redundancy on vessel-to-vessel air seeding and whole segment conductance and resistance to embolism spread. The objective of these simulations was to assess the role of vessel connectivity in overall segment safety, through P_{12}, P_{50}, P_{88}, and hydraulic efficiency, through $k_{xa,max}$.

In the simulations discussed below, pit membrane pore diameter, a, and b (equation 4) are fit to match *Acer glabrum var. glabrum*'s $k_{xa,max}$ and VC (Lens, Sperry, Christman, Choat, Rabaey, and Jansen, 2011; Mrad, Domec, Huang, Lens, and Katul, 2018, as in Fig. 1). However, the results are insensitive to the species used for initial fitting because they are presented in terms of normalized $k_{xa,max}$ and PLC measures, as explained in what follows.

4 Results

When VA_x^{-1} in a segment cross-section increased, GI and $\langle c \rangle$ increased (Fig. S2). In contrast, the model indicated that $\langle D_v \rangle$ and $\langle L_v \rangle$ had no influence on measures of connectivity. The effect of VA_x^{-1} on $\langle c \rangle$ is due to conduit placement throughout a cross-section being random. A point pattern analysis of three *Acer* species support this assumption (Martínez-Vilalta, Mencuccini, Álvarez, Camacho, Loepfe, and Piñol, 2012) and the anatomical measurements by Lens, Sperry, Christman, Choat, Rabaey, and Jansen (2011) show a strong correlation between VA_x^{-1} and GI, further corroborating this outcome. Conversely, While individual vessel length L_v is a strong predictor of the connectivity c of a single vessel, $\langle L_v \rangle$ in a xylem segment did not impact $\langle c \rangle$.

One of the hypothesized advantages of an increase in $\langle c \rangle$ is an increase in pathway redundancy, a measure of interest for many biological networks, including in the neurosciences and genetics (Tononi, Sporns, and Edelman, 1999). As $\langle c \rangle$ increased from small values, redundancy increased significantly through the avoidance of vessel isolation. But, redundancy reached a maximum and saturated at and above a critical value of $\langle c \rangle$. To quantify the pathway redundancy of a simulated xylem, the fraction of embolized vessels at complete hydraulic failure (PLC = 100) was used (Fig. 4a in orange). The rationale behind this metric is best explained through Fig. 3a, b: the xylem network with lower $\langle c \rangle$ has a higher proportion of isolated conduits compared to the one with higher $\langle c \rangle$ even though the same conduits are embolized. It is then said that the xylem network in Fig. 3b is less redundant than the one in Fig. 3a. Pathway redundancy is quantified by the fraction of embolized conduits at PLC = 100 because it takes a larger fraction of embolized conduits for complete hydraulic failure (Fig. 3). Higher redundancy is achieved by reducing the instances of vessel isolation as a result of embolism spread events. That is achieved by increasing $\langle c \rangle$, which decreases the probability of a group of vessels becoming disconnected from the segment inlet or outlet. The maximum pathway redundancy ($\approx$ 90 %) is achieved at $\langle c \rangle \approx 2.8$ on average and it stagnates with further increases in $\langle c \rangle$ (Fig. 4, top in orange).

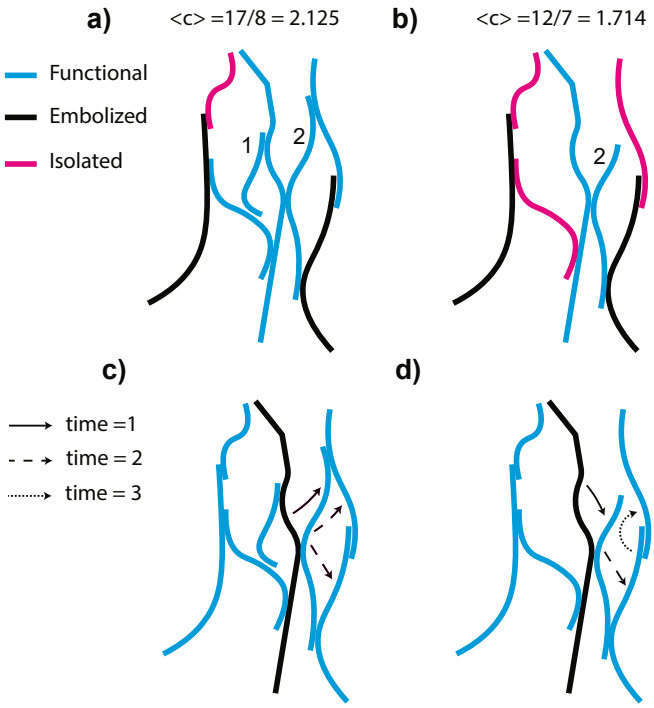

Fig. 3 Representation of how average conduit connectivity $\langle c \rangle$ affects redundancy (panels a and b) and embolism spread speed (panels c and d). $\langle c \rangle$ is calculated by counting the number of connections of each vessel and averaging. The xylem networks are similar for panels a and c and panels b and d, respectively. The difference between the two networks is that the conduit labeled "1" is present in panels a and c but not in panels b and d. The conduit labeled "2" is shorter in the latter panels and does not connect to the conduit on the top right. Panels a and b show how the network with lower $\langle c \rangle$ suffers from a greater number of isolated conduits than the network with higher $\langle c \rangle$. Conduit isolation occurs when a conduit still contains water but either the inlet or outlet is blocked by an embolized conduit. Panels c and d show how an embolism spreads faster in the network with higher $\langle c \rangle$ than the one with lower $\langle c \rangle$. The time step values in the legend are for illustration and are best understood as progressively increasing xylem water tension.

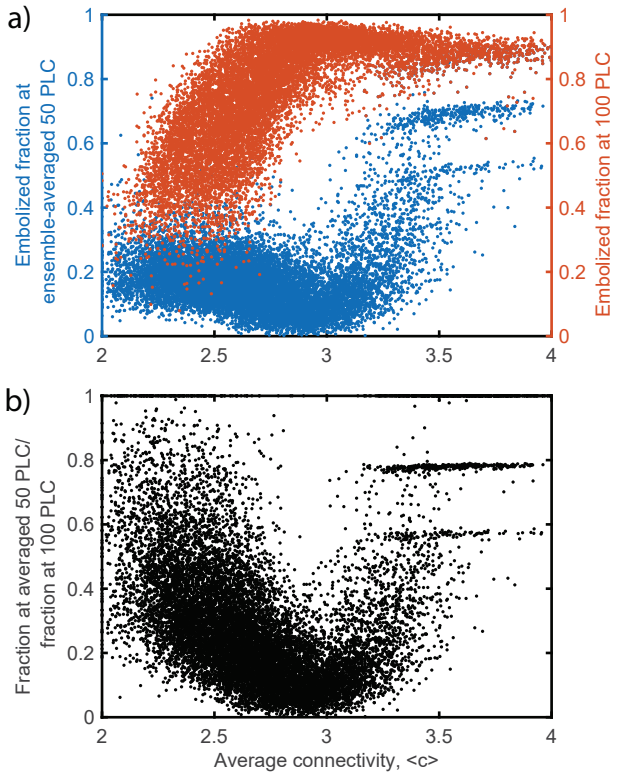

Fig. 4 The effect of average vessel connectivity $\langle c \rangle$ on pathway redundancy and embolism spread rate. a) embolism spread rate is quantified by the fraction of embolized vessels at the ensemble-averaged 50% loss of hydraulic conductivity (PLC; blue): average P_{50} of all simulations combined. Pathway redundancy is quantified by the fraction of embolized vessels at 100 PLC of each simulation (orange). b) embolism spread rate divided by pathway redundancy highlighting an optimal $\langle c \rangle$ at which embolism spread is minimized.

The hypothesized disadvantage of increased $\langle c \rangle$ is that it increases embolism spread speed with respect to P. $\langle c \rangle$ had minimal effect of spread speed until it reached a critical value. Above the critical value, embolism spread speed with respect to P increased dramatically. The effect of $\langle c \rangle$ on embolism spread was represented by the fraction of embolized vessels at the average P_{50} value (PLC = 50) of all simulations combined. By determining the fraction of embolized vessels at this common P, we compared the extent of embolism spread at the same pressure occuring at the steepest portion of the ensemble-averaged VC. This represents the speed of embolism spread with respect to increasing P. By plotting the value of this metric against $\langle c \rangle$ per simulation, it is observed that the minimum spread rate occurs around $\langle c \rangle = 3$ where about 10%, but as much as 20%, of all vessels are embolized (Fig. 4, a in blue).

Embolism spread speed in xylem is tied by analogy to the so-called bond percolation process. By leveraging this conceptual link, it is deduced that spread speed increases with $\langle c \rangle$ above $\langle c \rangle = 3$ because of a concomitant decrease in the percolation threshold ($F_{c,threshold}$). $F_{c,threshold}$ decreases from around 70% at $\langle c \rangle = 2$ to 35% at $\langle c \rangle = 3$ and further below as $\langle c \rangle$ increases (Fig. 5). The decrease in $F_{c,threshold}$ means that a smaller proportion of contact walls allowing embolism spread is required for a randomly placed embolism to propagate pervasively. This decline in $F_{c,threshold}$ explains the blow-up in the fraction of embolized vessels above $\langle c \rangle = 3$ (Fig. 4, a). Above $\langle c \rangle = 3$, $F_{c,threshold}$ declines below 35% and the blow-up in embolism spread speed happens (Figs. 4 and 5).

The distance between the embolism spread rate and pathway redundancy represents the safety of hydraulic conductance to embolism spread. This distance is evaluated by taking the ratio of these two model outputs (Fig. 4, b). This ratio is smallest when $\langle c \rangle$ is in the interval between 2.8 and 3 at about 10%. This analysis suggests that *Acer* species might conserve vessel connectivity, not GI (see below), to improve embolism resistance regardless of pit and vessel anatomy.

An increase in $\langle c \rangle$ to 3 increased P_{12} significantly but not P_{88}, imparting a smaller increase to P_{50} (Fig. 6). Above $\langle c \rangle$ to 3, P_{12}, P_{50}, and P_{88} decreased such that the redundancy-spread speed trade-off was corroborated. The ordinates in Fig. 6 are normalized by their respective simulation means. This is to isolate the effects of

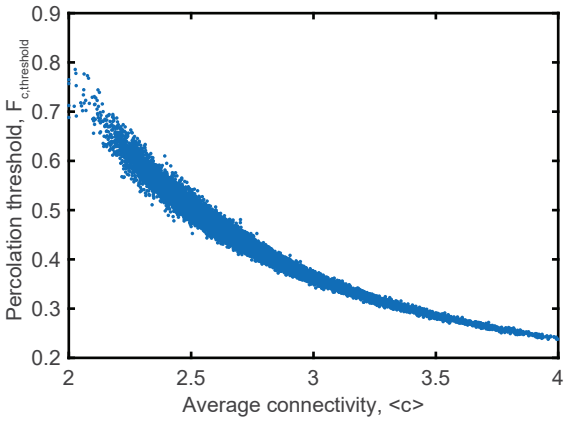

Fig. 5 The percolation threshold decreases with increasing average connectivity $\langle c \rangle$. The percolation threshold is a threshold fraction of conduit-to-conduit contact walls that allow an adjacent embolism to spread through them at a given xylem sap tension. If that threshold is exceeded, then a randomly placed embolism in the xylem network is expected to spread to the majority of the network.

$\langle c \rangle$ because the dimensional pressure values depend on pit membrane anatomy and frequency throughout vessel walls. An increase in $\langle c \rangle$ to 3 entailed an improvement in P_{12}, commonly referred to as the 'air-entry pressure'. In this case, variations in P_{12} are not related to air-seeding and air entry dynamics but the concept of redundancy (Fig. 4). Above $\langle c \rangle = 3$, gains in redundancy stagnated (Fig. 4) while the percolation threshold continued to decline (Fig. 5). Detrimental effects of a reduction in percolation threshold hold for P_{50} and P_{88} as well. In contrast, it appears from Fig. 6 that better embolism spread resistance due to redundancy is strongest in the low-pressure portion of VCs (i.e., P_{12}). Therefore, the effect of $\langle c \rangle$ on P_{88} is minimal below $\langle c \rangle = 3$. As a result, increases in P_{50} due to pathway redundancy were weaker compared to P_{12} but still present.

In contrast to $\langle c \rangle$, the effect of GI on VC measures was weaker. The simulation scatterplots showed P_{12} being significantly affected by GI whereas the relation of GI to P_{50} and P_{88} was nuanced (Fig. 7). Having low GI (≈ 1.5) did not preclude a high P_{12} but a high GI constrains P_{12} to higher values (Fig. 7,a). The *Acer* data conforms

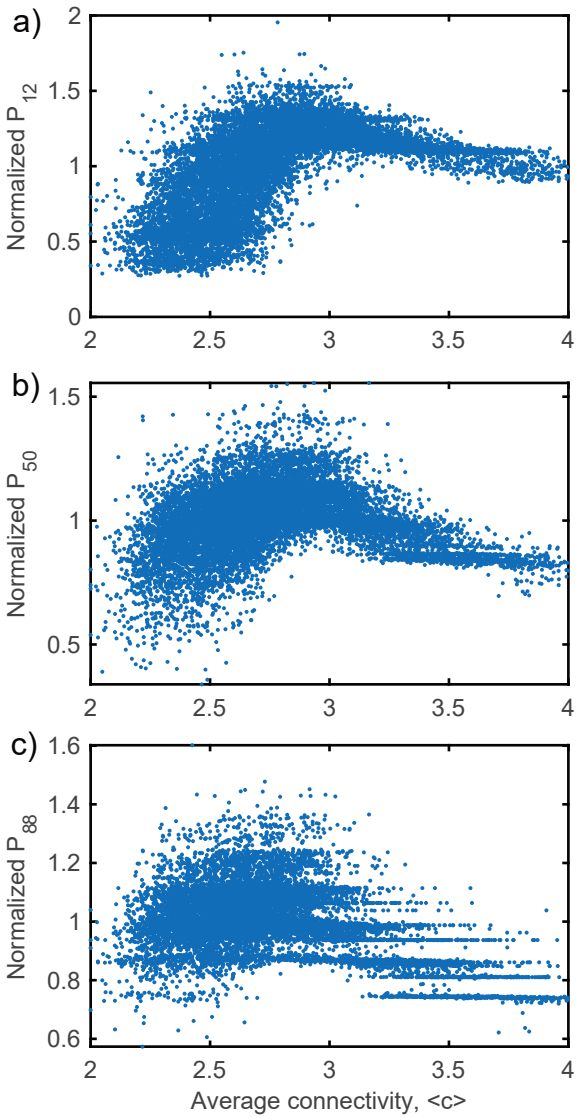

Fig. 6 The average vessel connectivity $\langle c \rangle$ affects a) P_{12} significantly, b) P_{50} mildly, and c) P_{88} minimally. The ordinates are normalized by the respective simulation means. The dimensional pressure values are a function of pit membrane anatomy and the average vessel wall area occupied by pit membranes. Since the interest here lies in the effect of $\langle c \rangle$ only, the ordinates are normalized.

to the scatter plot. The simulations show that P_{88} and GI were uncorrelated for the simulations leaving a weak relation between GI and P_{50} (Fig. 7,b,c).

The $\langle L_v \rangle$ is a strong predictor of maximum xylem area specific hydraulic conductivity ($k_{xa,max}$; Fig. 8) but not GI or $\langle D_v \rangle$, and therefore the lumen fraction F. As was done for P_{12}, P_{50}, and P_{88}, $k_{xa,max}$ is normalized by simulation and *Acer* dataset means appropriately (Fig. 8). The model correlation between $\langle L_v \rangle$ and $k_{xa,max}$ indicates that water movement through vessel wall pits is the most restrictive to overall sap flow (Choat, Cobb, and Jansen, 2008). With longer vessels, sap crosses a smaller number of pit membranes on average thus increasing the whole segment conductivity (Fig. 8, b). Over the ensemble of simulations, GI and $\langle D_v \rangle$ were weakly correlated with $k_{xa,max}$ (Fig. 8, a). In the *Acer* branches, GI and VA_x^{-1} are strongly correlated (Lens, Sperry, Christman, Choat, Rabaey, and Jansen, 2011). Since F in these branches is constrained to the range spanning 15% to 25% (Fig. S3), there exists a trade-off between vessel frequency per transverse area (VA_x^{-1}) and $\langle D_v \rangle$. This is because F is the fraction of the transverse stem area occupied by vessel lumen ($F = VA_x^{-1}(\pi/4)\langle D_v^2 \rangle$). As a result, it was hypothesized that increasing GI would lead to decreasing $k_{xa,max}$ due to a decrease $\langle D_v \rangle$ but this did not happen (Fig. 8, a). The $\langle L_v \rangle$-$k_{xa,max}$ relation was minimally affected when F was constrained in the model because $\langle L_v \rangle$ had the stronger effect on $k_{xa,max}$ than $\langle D_v \rangle$ (gray scatterplots; Fig. 8, b). Therefore, the presence of a correlation between GI and $k_{xa,max}$ in the *Acer* data (Lens, Sperry, Christman, Choat, Rabaey, and Jansen, 2011, Fig. 8, a) occurs because of a separate correlation between GI and $\langle L_v \rangle$ (Lens, Sperry, Christman, Choat, Rabaey, and Jansen, 2011).

5 Discussion

The simulations suggested that vessel connectivity and grouping improved segment-level resistance to embolism spread without affecting hydraulic conductivity. Increases in $\langle c \rangle$ and GI lead to an increase in P_{12} (more negative potential) through redundancy when all other anatomical features are held constant. There is a limit

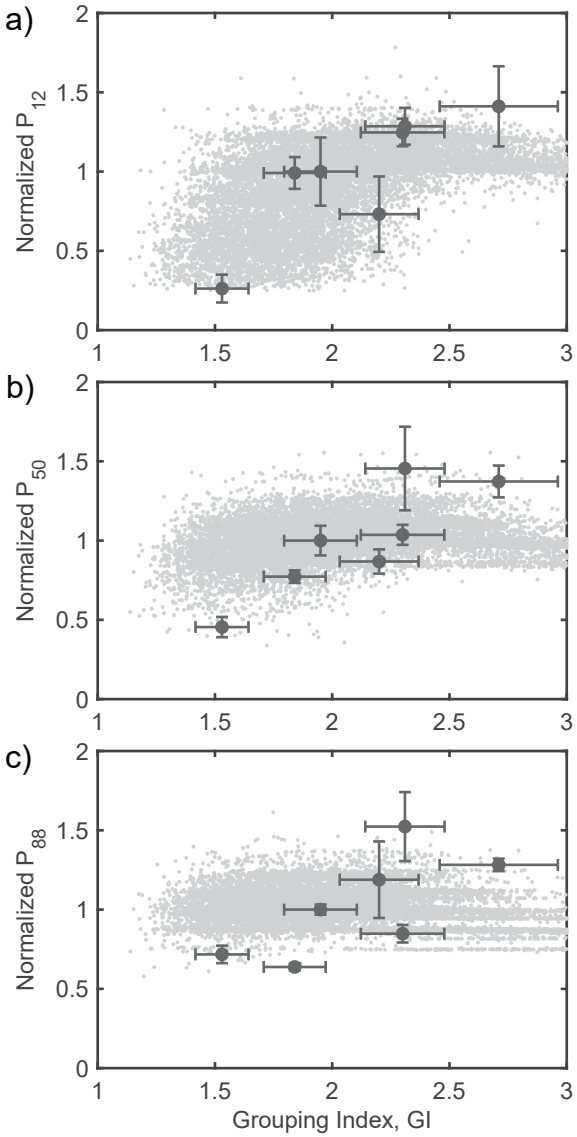

Fig. 7 The grouping index (GI) affects a) P_{12} significantly but its effect on b) P_{50} is nuanced while it bears no effect on c) P_{88}. The ordinates are normalized by the respective simulation or *Acer* data means. The simulations are shown in light gray while data derived from *Acer* vulnerability to embolism curves are in large symbols. The error bars around the *Acer* data points are standard errors from (Lens, Sperry, Christman, Choat, Rabaey, and Jansen, 2011).

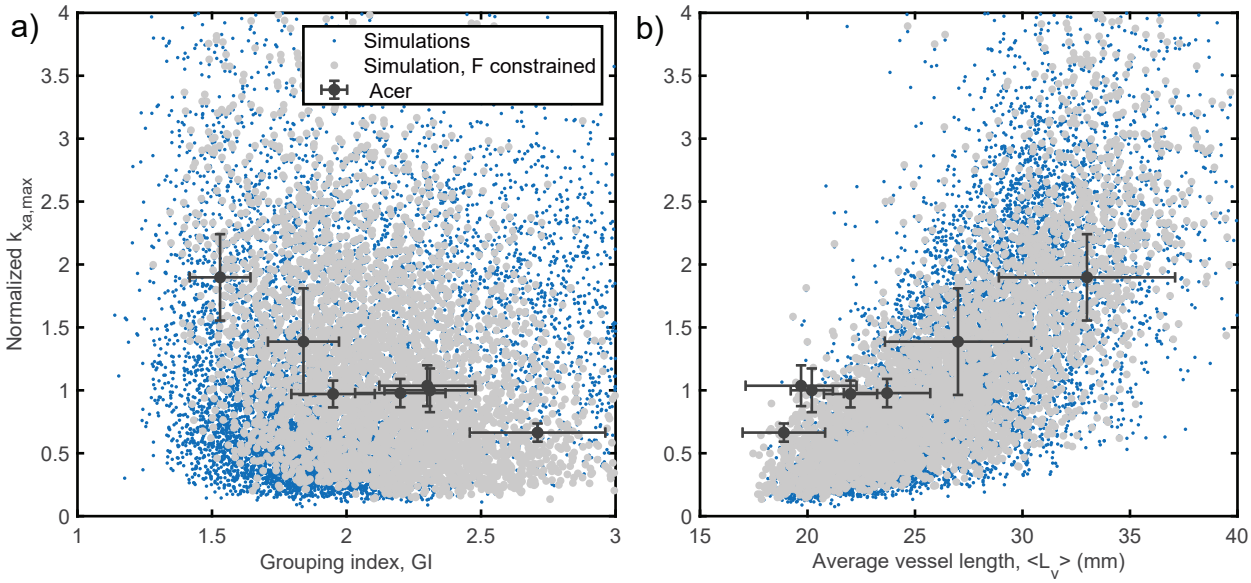

Fig. 8 While the *Acer* dataset (dark gray circles) shows significant correlations between the maximum xylem area specific hydraulic conductivity ($k_{xa,max}$) and the a) grouping index (GI) and the b) average vessel length ($\langle L_v \rangle$), simulations show that only $\langle L_v \rangle$ is a significant predictor of $k_{xa,max}$ (blue and light gray circles). The simulations vary properties pertinent to vessel anatomy and connectivity, but not pit membrane hydraulic properties (see Description). Light gray circles are scatter plots of simulations where the vessel lumen fraction is constrained to between 15% and 25% (Fig. S3). The error bars around the *Acer* data points are standard errors from (Lens, Sperry, Christman, Choat, Rabaey, and Jansen, 2011). On the ordinate is $k_{xa,max}$ normalized appropriately by simulation or dataset means.

to the positive relation between measures of vessel connection and P_{12} at $\langle c \rangle = 3$. At this value, embolism percolation dynamics overtook redundancy in influence but the *Acer* species did not seem to cross that limit. Increases in $\langle c \rangle$ below that limit increased P_{12} more strongly than P_{50} and P_{88}. As a result, higher vessel connectivity is thought to contribute to a steeper VC (Figs. 6 and 7).

One could also use the relation between $\langle c \rangle$ and redundancy to compare relative connectivities between species (Fig. 3). If one compares the proportion of air-filled conduits at a PLC ≈ 100 between different species, then one could infer that the species with the lowest proportion of embolized conduits is the least redundant and thus has lower $\langle c \rangle$. But to make an inference about relative differences in $\langle c \rangle$ between species based redundancy arguments, the species compared should all have only vessels as the main pathway for water and air-seeding the main mode of embolism spread in the xylem network.

Unfortunately, there does not exist data on *Acer* vessel connectivity in the literature due to the labor-intensive nature of these measurements. Consequently, we relied on a closely related measure, GI, which is reported for the *Acer* species (Lens, Sperry, Christman, Choat, Rabaey, and Jansen, 2011). GI is a two-dimensional measure of vessel connection. Fig. 9 shows the relation between the average transverse vessel connectivity $\langle c_x \rangle$ and GI. $\langle c_x \rangle$ quantifies only the connectivity apparent from a transverse stem section. So, it is the two-dimensional equivalent of $\langle c \rangle$. The $\langle c_x \rangle$ and GI differ if the fraction of tangential vessel connections varies from species to species as seen by comparing Fig. 9b and Fig. 9c. While Fig. 9b and Fig. 9c have the same GI, the latter has a higher $\langle c_x \rangle$. Therefore, when vessel connections have a preferred direction (radial in *Acer*), they limit $\langle c_x \rangle$ and, therefore, $\langle c \rangle$ to lower values for the same GI. It is typical to have conduit connections in a predominantly preferred direction in angiosperm xylem with only vessels as the water pathway. One possible driver of this trend is the potential increase in the 'air-entry' pressure of xylem (P_{12}) due to increases in GI (Fig. 7, a) while maintaining a high percolation threshold (Fig. 5) by maintaining $\langle c \rangle$ to values low enough to prevent the blowup in embolism spread speed (Fig. 4). This supports the hypothesis that increasing GI is a necessary but insufficient condition to improve *Acer* resistance to embolism

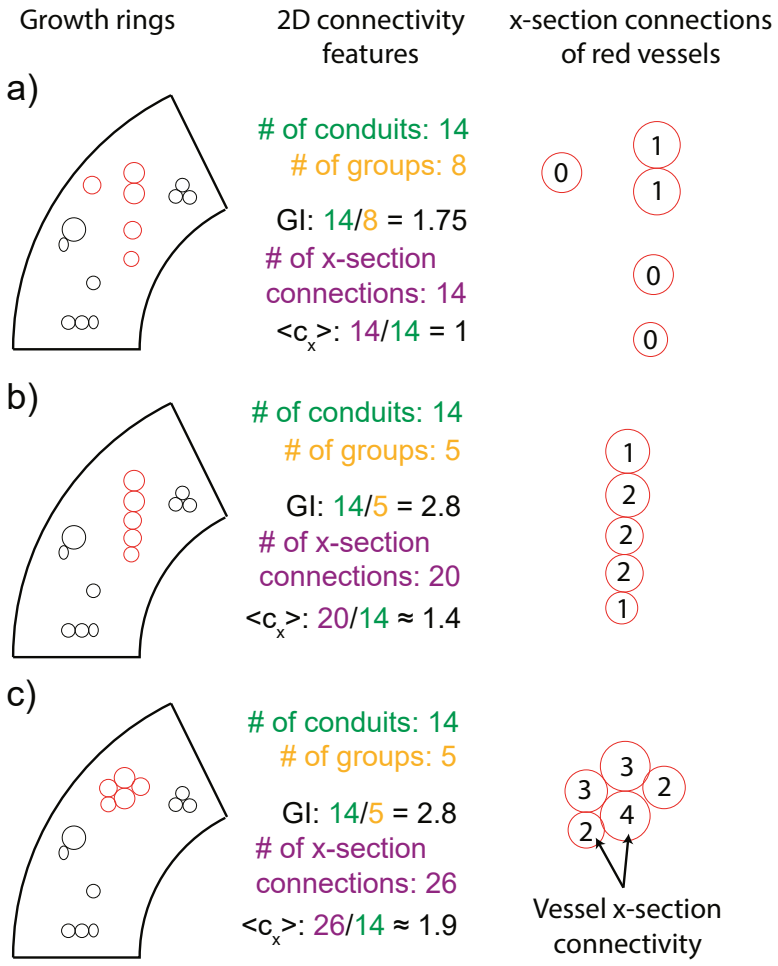

Fig. 9 Illustration showing the discrepancy between the grouping index (GI) and transverse or cross-section (x-section) vessel connectivity $\langle c_x \rangle$. The GI is defined as the number of vessels (number in green) divided by the number of vessel groups (number in orange). The $\langle c_x \rangle$ is the number of cross-section vessel connections (number in purple) divided by the number of vessels in a transverse stem section. The vessels in black are invariant whereas those in red form different vessel multiples when comparing a), b), and c). On the right-most column, the red vessels are highlighted and the cross-sectional connectivity $langlec_x$ of each is written inside of it. The "# of x-section connections" in the middle column is the sum of the vessel connectivities in the growth rings (left column) for both the black and red vessels. Especially when comparing b) and c), we see that 1 vessel group can have a higher connectivity with more tangential connections. While the illustrations in this figure are constrained to the cross-section, the same concepts apply in 3 dimensions with the 3-dimensional vessel connectivity property $\langle c \rangle$.

spread.

Nonetheless, trends between GI and PLC measures are similar, but weaker, to those with $\langle c \rangle$ despite having varied the fraction of tangential and diagonal connections four-fold in the simulations (Fig. 7 and S1). Most striking is the absence of a linear relation between GI and P_{50} but its presence in the *Acer* dataset (Lens, Sperry, Christman, Choat, Rabaey, and Jansen, 2011). This suggests that the trend seems to stem from the significant correlation between GI and another pit membrane property. This assertion is corroborated by a linear relation between GI and P_{88} in the dataset (Fig. 7b). Indeed, in the *Acer* data (Lens, Sperry, Christman, Choat, Rabaey, and Jansen, 2011), T_m has been shown to be a strong predictor of resistance to embolism spread at the pit and vessel levels (Li, Lens, Espino, Karimi, Klepsch, Schenk, Schmitt, Schuldt, and Jansen, 2016) and at the xylem segment level (Lens, Sperry, Christman, Choat, Rabaey, and Jansen, 2011). In a recent study on Poplar, embolism resistance plasticity in *Populus tremula x alba* has shown a strong correlation between GI and P_{50} (Lemaire, Quilichini, Brunel-Michac, Santini, Berti, Cartailler, Conchon, Badel, and Herbette, 2021). Concurrently, *Populus tremula x alba*, a member of the Salicaceae family that largely does not possess vasicentric tracheids, has shown a significant decrease in the pit membrane area per vessel with an increase in P_{50}. These empirical examples support the hypothesis that GI is necessary for embolism spread resistance in such angiosperm families but needs to be accompanied by variations in pit and vessel anatomy.

If increasing $\langle c \rangle$ leads to improved xylem resistance to embolism spread without negatively affecting hydraulic flow efficiency, then what might the evolutionary drivers of $\langle c \rangle$ variation between species be? The fact that the ubiquitous GI measurements could be uncorrelated to measures of 3D connectivity (Fig. 9) means that, currently, the data needed to answer this question are unavailable. If, however, $\langle c \rangle$ is correlated with GI and air-seeding is the main way for embolisms to spread, then species such as those in the *Acer* genus might have to increase $\langle c \rangle$ at the expense of increasing vessel frequency. This is because GI and VA_x^{-1} are highly correlated in *Acer* (Lens, Sperry, Christman, Choat, Rabaey, and Jansen, 2011). This would incur one of two costs: Either there would be less space for other types of cells in

the xylem like fibers and parenchyma, negatively affecting biomechanics and storage ((Pratt and Jacobsen, 2017)), or the conduits would have smaller diameters to preserve space with implications for hydraulic efficiency and construction costs in terms of carbon (Fig. S2). The latter is what is observed in the set of *Acer* species where a near-constant vessel packing fraction is conserved (Fig. S3; Lens, Sperry, Christman, Choat, Rabaey, and Jansen, 2011). However, reliable, inter-family measurements of $\langle c \rangle$ are necessary to validate or correct this hypothesis.

Resistance to embolism spread in plant organs is determined by the intersection among multiple anatomical traits operating at different scales. The ultra-structure of pit membranes determines the size of the nanopores that both allow water flow and restrict embolism spread (Jansen, Choat, and Pletsers, 2009; Lens, Sperry, Christman, Choat, Rabaey, and Jansen, 2011; Li, Lens, Espino, Karimi, Klepsch, Schenk, Schmitt, Schuldt, and Jansen, 2016; Zhang et al., 2020). Wider vessels reduce water flow resistance but a larger surface area, with more pit membranes, has been suggested to facilitate embolism spread (Hargrave, Kolb, F. Ewers, and Davis, 1994; Christman, Sperry, and Adler, 2009; Christman, Sperry, and Smith, 2012). A common theme among these traits, when they change, is that they affect k_{xa} and P_{50} in opposing ways. This reason is partly behind the expectation that safe species, with high resistance to drought, are less efficient with low hydraulic conductivity, and vice versa. This expectation leads to the hypothesis of the 'safety-efficiency' trade-off (Tyree, Davis, and Cochard, 1994) which has recently been shown to be weak (Gleason, Westoby, Jansen, Choat, Hacke, Pratt, Bhaskar, Brodribb, Bucci, Cao, et al., 2016). However, the simulations perturbing vessel connectivity have shown that it has a significant effect on the slope of the VC (Fig. 6 and 7) regardless of changes in pit and vessel anatomy. These 'middle-scale' variations in xylem networks do not affect P_{50} and $k_{xa,max}$, typical measures of xylem safety and efficiency, in clearly opposing ways (Manzoni, Vico, Katul, Palmroth, Jackson, and Porporato, 2013). The weakness of the expected safety-efficiency trade-off among woody species (Gleason, Westoby, Jansen, Choat, Hacke, Pratt, Bhaskar, Brodribb, Bucci, Cao, et al., 2016) might be because an increase in vessel connectivity, all else constant, could improve P_{50} (to a certain extent; Fig/ 6,b) while not affecting $k_{xa,max}$ (as observed through

the 2D proxy GI, blue and gray scatter plots in Fig. 8,a), unlike how changes in other anatomical traits affect them. doc

'Middle-scale' variations encompass more than trends in vessel grouping, especially in flowering plans with vasicentric tracheids (Carlquist, 1984; Carlquist, 2009). In such species, much of the hydraulic connectivity between vessels is mediated by radial or tangential bands of conductive tracheids. As a result, such species with mostly solitary vessels will encounter different embolism spread dynamics. A recent study on three flowering species with mostly solitary vessels has concluded that solitary cavitation events dominate over events that involve groups of vessels (Johnson, Brodersen, Carins-Murphy, Choat, and Brodribb, 2020). Consequently, species possessing different patterns of vessel connectivity will not conform to similar P_{50} and $k_{xa,max}$ trade-offs even if vessel and pit anatomy are identical.

In *Acer*, increasing conduit connectivity improves branch resistance to embolism spread without adversely affecting hydraulic conductivity. This may be true for all plants with vessels as the only water conducting cell type such as *Acer*. In general, that means that when xylem network characteristics vary among woody species, the 'safety-efficiency' trade-off hypothesis applied to the segment level might not hold. This result was established using a combination of numerical simulations and theoretical tactics borrowed from network and percolation theory. Increasing average conduit connectivity invoked a trade-off between hydraulic pathway redundancy and embolism spread speed with respect to pressure. Pathway redundancy increased with conduit connectivity because conduit isolation was avoided. Above a critical conduit connectivity, improvements in redundancy were canceled by embolism spread speed due to a declining percolation threshold. These results underscore the need to account for changes in average conduit connectivity, preferential arrangements, and cell types among organs and species to successfully generalize hydraulic trends.

6 Acknowledgments

AM acknowledges funding from the National Science Foundation (NSF-AGS-1644382, NSF-AGS-2028633). AM, DMJ, DML, and J-CD acknowledge the NSF for grant NSF-IOS-1754893. The authors appreciate the critical feedback provided by Dr. Gabriel G. Katul and Dr. Frederic Lens.

7 Author contributions

AM planned and designed the research and developed the computational model and the theory. AM, DMJ, DML, and J-CD analysed the data and model results and wrote the manuscript.

8 Data availability

Branch anatomy data on the seven *Acer* species were obtained Lens, Sperry, Christman, Choat, Rabaey, and Jansen (2011) after contacting the corresponding author of that study. The code for the model is found at https://github.com/mradassaad.

References

[1] DS Callaway, MEJ Newman, SH Strogatz, and DJ Watts. "Network robustness and fragility: Percolation on random graphs". In: *Physical Review Letters* 85.25 (2000), pp. 5468–5471.

[2] S Carlquist. "Vessel grouping in dicotyledon wood: significance and relationship to imperforate tracheary elements". In: *Aliso: A Journal of Systematic and Evolutionary Botany* 10.4 (1984), pp. 505–525.

[3] S Carlquist. "Non-random vessel distribution in woods: patterns, modes, diversity, correlations". In: *Aliso: A Journal of Systematic and Evolutionary Botany* 27.1 (2009), pp. 39–58.

[4] B Choat, AR Cobb, and S Jansen. "Structure and function of bordered pits: new discoveries and impacts on whole-plant hydraulic function". In: *New Phytologist* 177.3 (2008), pp. 608–626.

[5] MA Christman, JS Sperry, and FR Adler. "Testing the 'rare pit'hypothesis for xylem cavitation resistance in three species of Acer". In: *New Phytologist* 182.3 (2009), pp. 664–674.

[6] MA Christman, JS Sperry, and DD Smith. "Rare pits, large vessels and extreme vulnerability to cavitation in a ring-porous tree species". In: *New Phytologist* 193.3 (2012), pp. 713–720.

[7] H Cochard, P Cruiziat, and MT Tyree. "Use of positive pressures to establish vulnerability curves: further support for the air-seeding hypothesis and implications for pressure-volume analysis". In: *Plant Physiology* 100.1 (1992), pp. 205–209.

[8] R Cohen, K Erez, D Ben-Avraham, and S Havlin. "Resilience of the internet to random breakdowns". In: *Physical Review Letters* 85.21 (2000), pp. 4626–4628.

[9] HH Dixon and J Joly. "On the ascent of sap". In: *Philosophical Transactions of the Royal Society of London. B* 186 (1895), pp. 563–576.

[10] J-C Domec and BL Gartner. "Cavitation and water storage capacity in bole xylem segments of mature and young Douglas-fir trees". In: *Trees* 15.4 (2001), pp. 204–214.

[11] FW Ewers, JM Ewers, AL Jacobsen, and J López-Portillo. "Vessel redundancy: modeling safety in numbers". In: *IAWA Journal* 28.4 (2007), pp. 373–388.

[12] SM Gleason, M Westoby, S Jansen, B Choat, UG Hacke, RB Pratt, R Bhaskar, TJ Brodribb, SJ Bucci, K-F Cao, et al. "Weak tradeoff between xylem safety and xylem-specific hydraulic efficiency across the world's woody plant species". In: *New Phytologist* 209.1 (2016), pp. 123–136.

[13] UG Hacke, AL Jacobsen, and RB Pratt. "Xylem function of arid-land shrubs from California, USA: an ecological and evolutionary analysis". In: *Plant, Cell & Environment* 32.10 (2009), pp. 1324–1333.

[14] UG Hacke, JS Sperry, JK Wheeler, and L Castro. "Scaling of angiosperm xylem structure with safety and efficiency". In: *Tree Physiology* 26.6 (2006), pp. 689–701.

[15] KR Hargrave, KJ Kolb, FW Ewers, and SD Davis. "Conduit diameter and drought-induced embolism in Salvia mellifera Greene (Labiatae)". In: *New Phytologist* 126.4 (1994), pp. 695–705.

[16] T Hölttä, T Vesala, and E Nikinmaa. "A model of bubble growth leading to xylem conduit embolism". In: *Journal of Theoretical Biology* 249.1 (2007), pp. 111–123.

[17] AL Jacobsen and RB Pratt. "Going with the flow: Structural determinants of vascular tissue transport efficiency and safety". In: *Plant, Cell & Environment* 41.12 (2018), pp. 2715–2717.

[18] S Jansen, B Choat, and A Pletsers. "Morphological variation of intervessel pit membranes and implications to xylem function in angiosperms". In: *American Journal of Botany* 96.2 (2009), pp. 409–419.

[19] KM Johnson, C Brodersen, MR Carins-Murphy, B Choat, and TJ Brodribb. "Xylem embolism spreads by single-conduit events in three dry forest angiosperm stems". In: *Plant Physiology* 184.1 (2020), pp. 212–222.

[20] L Kaack, CM Altaner, C Carmesin, A Diaz, M Holler, C Kranz, G Neusser, M Odstrcil, HJ Schenk, V Schmidt, et al. "Function and three-dimensional structure of intervessel pit membranes in angiosperms: a review". In: *IAWA Journal* 40.4 (2019), pp. 673–702.

[21] M Kanduč, E Schneck, P Loche, S Jansen, HJ Schenk, and RR Netz. "Cavitation in lipid bilayers poses strict negative pressure stability limit in biological liquids". In: *Proceedings of the National Academy of Sciences* 117.20 (2020), pp. 10733–10739.

[22] W Konrad, G Katul, A Roth-Nebelsick, and KH Jensen. "Xylem functioning, dysfunction and repair: a physical perspective and implications for phloem transport". In: *Tree Physiology* 39.2 (2019), pp. 243–261.

[23] W Konrad and A Roth-Nebelsick. "The dynamics of gas bubbles in conduits of vascular plants and implications for embolism repair". In: *Journal of Theoretical Biology* 224.1 (2003), pp. 43–61.

[24] C Lemaire, Y Quilichini, N Brunel-Michac, J Santini, L Berti, J Cartailler, P Conchon, É Badel, and S Herbette. "Plasticity of the xylem vulnerability to embolism in Populus tremula x alba relies on pit quantity properties rather than on pit structure". In: *Tree Physiology* (Feb. 2021). tpab018. ISSN: 1758-4469. DOI: 10.1093/treephys/tpab018. eprint: https://academic.oup.com/treephys/advance-article-pdf/doi/10.1093/treephys/tpab018/36971185/tpab018.pdf. URL: https://doi.org/10.1093/treephys/tpab018.

[25] F Lens, JS Sperry, MA Christman, B Choat, D Rabaey, and S Jansen. "Testing hypotheses that link wood anatomy to cavitation resistance and hydraulic conductivity in the genus Acer". In: *New Phytologist* 190.3 (2011), pp. 709–723.

[26] S Li, F Lens, S Espino, Z Karimi, M Klepsch, HJ Schenk, M Schmitt, B Schuldt, and S Jansen. "Intervessel pit membrane thickness as a key determinant of embolism resistance in angiosperm xylem". In: *IAWA Journal* 37.2 (2016), pp. 152–171.

[27] L Loepfe, J Martinez-Vilalta, J Pinol, and M Mencuccini. "The relevance of xylem network structure for plant hydraulic efficiency and safety". In: *Journal of Theoretical Biology* 247.4 (2007), pp. 788–803.

[28] S Manzoni, G Vico, G Katul, S Palmroth, RB Jackson, and A Porporato. "Hydraulic limits on maximum plant transpiration and the emergence of the safety–efficiency trade-off". In: *New Phytologist* 198.1 (2013), pp. 169–178.

[29] J Martínez-Vilalta, M Mencuccini, X Álvarez, J Camacho, L Loepfe, and J Piñol. "Spatial distribution and packing of xylem conduits". In: *American Journal of Botany* 99.7 (2012), pp. 1189–1196.

[30] A Mrad, J-C Domec, C-W Huang, F Lens, and G Katul. "A network model links wood anatomy to xylem tissue hydraulic behaviour and vulnerability to cavitation". In: *Plant, Cell & Environment* 41.12 (2018), pp. 2718–2730.

[31] MEJ Newman. *Networks*. Oxford university press, 2018.

[32] RB Pratt and AL Jacobsen. "Conflicting demands on angiosperm xylem: Trade-offs among storage, transport and biomechanics". In: *Plant, Cell & Environment* 40.6 (2017), pp. 897–913.

[33] RB Pratt and AL Jacobsen. "Identifying which conduits are moving water in woody plants: a new HRCT-based method". In: *Tree Physiology* 38.8 (2018), pp. 1200–1212.

[34] RB Pratt, MI Percolla, and AL Jacobsen. "Integrative Xylem Analysis of Chaparral Shrubs". In: *Functional and Ecological Xylem Anatomy*. Ed. by Uwe Hacke. Cham, Switzerland: Springer International Publishing, 2015, pp. 189–207. ISBN: 978-3-319-15783-2. DOI: 10.1007/978-3-319-15783-2_7.

[35] A Roth-Nebelsick. "It's contagious: calculation and analysis of xylem vulnerability to embolism by a mechanistic approach based on epidemic modeling". In: *Trees* 33.5 (2019), pp. 1519–1533.

[36] S Salleo, TM Hinckley, SB Kikuta, MA Lo Gullo, P Weilgony, T-M Yoon, and H Richter. "A method for inducing xylem emboli in situ: experiments with a field-grown tree". In: *Plant, Cell & Environment* 15.4 (1992), pp. 491–497.

[37] Y Sano, H Morris, H Shimada, LP Ronse De Craene, and S Jansen. "Anatomical features associated with water transport in imperforate tracheary elements of vessel-bearing angiosperms". In: *Annals of Botany* 107.6 (2011), pp. 953–964.

[38] HJ Schenk, S Espino, DM Romo, N Nima, AYT Do, JM Michaud, B Papahadjopoulos-Sternberg, J Yang, YY Zuo, K Steppe, et al. "Xylem surfactants introduce a new element to the cohesion-tension theory". In: *Plant Physiology* 173.2 (2017), pp. 1177–1196.

[39] HJ Schenk, K Steppe, and S Jansen. "Nanobubbles: a new paradigm for air-seeding in xylem". In: *Trends in Plant Science* 20.4 (2015), pp. 199–205.

[40] JS Sperry and NZ Saliendra. "Intra-and inter-plant variation in xylem cavitation in Betula occidentalis". In: *Plant, Cell & Environment* 17.11 (1994), pp. 1233–1241.

[41] JS Sperry and MT Tyree. "Mechanism of water stress-induced xylem embolism". In: *Plant Physiology* 88.3 (1988), pp. 581–587.

[42] G Tononi, O Sporns, and GM Edelman. "Measures of degeneracy and redundancy in biological networks". In: *Proceedings of the National Academy of Sciences* 96.6 (1999), pp. 3257–3262.

[43] MT Tyree, SD Davis, and H Cochard. "Biophysical perspectives of xylem evolution: is there a tradeoff of hydraulic efficiency for vulnerability to dysfunction?" In: *IAWA Journal* 15.4 (1994), pp. 335–360.

[44] MT Tyree and MH Zimmermann. *Xylem Structure and the Ascent of Sap*. Springer Series in Wood Science. Springer, 2002. ISBN: 9783540433545.

[45] MD Venturas, RB Pratt, AL Jacobsen, V Castro, JC Fickle, and UG Hacke. "Direct comparison of four methods to construct xylem vulnerability curves: Differences among techniques are linked to vessel network characteristics". In: *Plant, Cell & Environment* 42.8 (2019), pp. 2422–2436.

[46] MD Venturas, JS Sperry, and UG Hacke. "Plant xylem hydraulics: what we understand, current research, and future challenges". In: *Journal of Integrative Plant Biology* 59.6 (2017), pp. 356–389.

[47] Y Zhang et al. "High porosity with tiny pore constrictions and unbending pathways characterize the 3D structure of intervessel pit membranes in angiosperm xylem". In: *Plant, Cell & Environment* 43.1 (2020), pp. 116–130.

Fig. S1: The probability of tangential inter-vessel connections does not explain variation in kxa, max and b) P_{50}.

Fig. S2: The effect of VA_x^{-1} on a) GI and b) c.

753 **Fig. S3**: The seven Acer species maintain a tight relation between VA_x^{-1} and
754 average vessel lumen area.

755 **Description S1**: Modeling xylem networks: sap flow

756 **Description S2**: Calculating GI and VA_x^{-1} in the model